Journal of
Engineering Sciences
Faculty of Engineering
Assiut University
JES
مجلة
العلوم الهندسية
كلية الهندسة
جامعة أسيوط
journal homepage: http://jesaun.journals.ekb.eg

Spatio-Temporal Modeling of Near-Surface Air Temperature Based on Satellite-Derived LST in the Mediterranean Region, Türkiye

Received 18 September 2025; Revised 4 February 2026; Accepted 4 February 2026

Nihat Karakuş[1]*
Serdar Selim[2]
Burçin Dönmez[3]
Ali Kılçık[4]
Rifat Olgun[5]
Meliha Aklıbaşında[6]
Emine Kahraman[7]

Keywords
Climate change; Land surface temperature; Linear regression; Pearson correlation; Estimate near-surface air temperature.

Abstract: Accurate estimation of near-surface air temperature (Ta-est) is of great importance, particularly in regions characterized by complex land cover and sparse meteorological station networks. Although meteorological station measurements provide high temporal accuracy, interpolation approaches limited by station density and distribution cannot adequately represent microclimatic variability under heterogeneous land conditions. To overcome these limitations, this study estimates air temperature at the pixel scale by modeling land surface temperature (LST) derived from high-resolution Landsat 8 satellite imagery together with air temperature measurements (Ta) obtained from meteorological stations. The analysis is based on monthly Landsat 8 data for the 2016–2019 period and air temperature observations from 11 meteorological stations. To model the LST–Ta relationship, linear, logarithmic, exponential, and second-order polynomial regression models were developed, and their performances were evaluated using RMSE, MBE, and R^2 metrics. The results demonstrate that the linear regression model exhibits a more balanced and generalizable performance than the other models, characterized by consistently low error levels, negligible bias, and stable explanatory power throughout the year. While all models show high explanatory capability during winter months, performance declines are observed in the nonlinear models during summer and transitional seasons due to increasing heterogeneity in surface–atmosphere energy exchanges. The Ta-est maps generated using the linear regression model show a strong correlation with observed Ta values, with absolute differences predominantly remaining below 1 °C. Overall, the methodology and findings of this study demonstrate that microclimatic variability can be successfully modeled and provide a practical framework for producing spatially detailed air temperature datasets.

[1] nkarakus@akdeniz.edu.tr , Dr. Lecturer, Department of Park and Horticulture, Vocational School of Serik G-S. Sural, Akdeniz University, 07500 Antalya, Türkiye.
[2] serdarselim@akdeniz.edu.tr , Associate Professor, Department of Space Sciences and Technologies, Faculty of Science, Akdeniz University, 07070 Antalya, Türkiye.
[3] burcindonmez@akdeniz.edu.tr , Assist. Professor, Department of Space Sciences and Technologies, Faculty of Science, Akdeniz University, 07070 Antalya, Türkiye.
[4] alikilcik@akdeniz.edu.tr , Professor, Department of Space Sciences and Technologies, Faculty of Science, Akdeniz University, 07070 Antalya, Türkiye.
[5] rifatolgun@akdeniz.edu.tr , Associate Professor, Department of Park and Horticulture, Vocational School of Serik G-S. Sural, Akdeniz University, 07500 Antalya, Türkiye.
[6] melihaaklibasinda@nevsehir.edu.tr , Associate Professor, Department of Landscape Architecture, Faculty of Engineering and Architecture, Nevşehir Haci Bektaş Veli University, 50300 Nevşehir, Türkiye;
[7] eminekahraman@akdeniz.edu.tr , Dr. Lecturer, Department of Park and Horticulture, Vocational School of Serik G-S. Sural, Akdeniz University, 07500 Antalya, Türkiye.

https://doi.org/10.21608/JESAUN.2026.425073.1742
This is an open access article under the CC BY-NC-ND license (http://creativecommons.org/licenses/by-nc-nd/4.0/).

1. Introduction

Air Near-surface air temperature (Ta) is a fundamental climatic variable that directly or indirectly influences a wide range of physical and biological processes occurring within the hydrosphere, lithosphere, and biosphere, spanning from atmospheric circulation processes to ecosystem functioning [1,2,3]. Since Ta plays a critical role in surface–atmosphere energy balance, evaporation and evapotranspiration processes, and biological productivity, it is widely used in studies involving climate analysis, environmental assessment, and human–environment interactions [1,4,5]. In particular, Ta data, characterized by high spatial resolution and spatial continuity, not only enable more accurate analysis of climatic processes but also constitute essential input data for scientific studies conducted across diverse disciplines such as environmental sciences, agriculture, hydrology, ecology, and tourism [4,6,7]. In this context, determining air temperature with high accuracy at different spatial scales increases the reliability of climatic analyses and directly affects the validity and applicability of the scientific outputs produced [8,9].

Conventional air temperature data are based on thermometer measurements conducted at fixed or mobile terrestrial meteorological stations in accordance with the measurement standards and observational principles defined by the World Meteorological Organization (WMO) [3,10,11,12]. Although this approach provides high accuracy at the point scale and strong temporal resolution, the spatial representativeness of the measurements is often limited to the surrounding area of the station [8,11,13]. At locations distant from meteorological stations, temperature values vary considerably as a function of differences in topography, land cover, and urban morphology [12,14,15]. For this reason, particularly in urban areas and rural regions characterized by complex land-use patterns, it becomes difficult for a single fixed station to fully represent local climatic conditions [2,13]. Therefore, assessments based solely on station data are insufficient to adequately capture microclimatic differences in regions with heterogeneous topography and land cover [14,16].

This limitation in temperature data is commonly addressed through the application of spatial interpolation methods [16,17,18]. However, in local climate regions characterized by sparse meteorological station networks and high topographic and land-cover heterogeneity, air temperature datasets derived solely from station-based interpolation do not always provide the level of accuracy and spatial detail required by decision-makers [8,14]. The accuracy of interpolation results is generally affected by factors such as station density, station location, and the heterogeneity of the region being studied [16,19]. The literature emphasizes that mobile measuring stations or remote sensing technologies should be used to reliably map temperatures in regions with heterogeneous topography and insufficient numbers of stations [5,14,15]. In this context, it is necessary to establish networks of meteorological stations that are close to each other in terms of distance in order to obtain reliable Ta data at the micro, local, and meso scales [16,17,19,20]. However, since the establishment and maintenance of such a network of stations involves high costs and logistical challenges, estimating Ta from satellite imagery has become an important alternative in regions where station density is insufficient [3,18,21,22,23,24]. The analysis of satellite images equipped with TIR bands using Geographic Information Systems (GIS) enables the processing of LST at the pixel scale, thereby producing pixel-based temperature data across large areas [5,25,26,27,28]. In this way, representativeness issues arising from the point-based nature of station measurements can be reduced to a certain extent [14,27].

Satellite-based remote sensing data are frequently used in studies focusing on climate, environmental processes, and land–atmosphere interactions, owing to their capacity to produce spatially continuous distributions of climatic variables over large areas and to represent these variables at multiple spatial scales [5,27,29,30,31,32]. LST is a fundamental remote sensing variable widely used in understanding surface-

atmosphere interactions and in estimating near-surface air temperature (Ta) [33,34,35,36]. In the literature, it is observed that MODIS data with a spatial resolution of 1 × 1 km are mostly preferred in modeling the relationship between LST and near-surface air temperature [6,14,23,37]. The high temporal resolution and broad spatial coverage of MODIS sensors provide significant advantages for monitoring temperature patterns at regional and global scales [20,38]. However, the relatively coarse spatial resolution of MODIS data limits the detailed characterization of microclimatic variability, particularly in urban areas with high land-cover heterogeneity and in regions with complex topography [2,9]. This limitation increases the need for higher spatial resolution data in analyses of urban heat island effects, local temperature gradients, and small-scale thermal variability [5]. In this context, interest in LST studies based on Landsat 8 satellite imagery has increased substantially in recent years [30,39]. LST data derived from Landsat 8 imagery, where the thermal band originally acquired at 100 m spatial resolution is resampled and distributed at 30 m by the USGS, enable a more detailed pixel-scale representation of LST [25,30,32]. This high spatial resolution allows for more precise air temperature estimation from LST and provides a significant advantage in identifying local temperature differences [23,39]. Owing to this enhanced spatial detail, Landsat 8-based studies not only improve estimation accuracy but also enable the detection of microclimatic patterns that cannot be resolved in MODIS-based analyses [5,40,41,42]. Particularly in regions characterized by heterogeneous urban fabrics and complex topographic conditions, Landsat-based LST analyses offer a strong alternative for local climate assessments and decision-support processes [41].

Studies aimed at estimating air temperature (Ta) from both Landsat- and MODIS-based LST data have widely employed linear, logarithmic, exponential, and polynomial regression models, as well as multivariate statistical approaches and machine learning-based methods [15,23,33,41]. Among these methods, linear regression models are the most commonly used approach for characterizing the LST-Ta relationship [34,37,43]. Owing to their simple structure, low data requirements, and physical interpretability, linear models have been frequently preferred in both MODIS- and Landsat-based studies [10,44,45]. The performance of Ta estimation models has generally been evaluated using error metrics such as root mean square error (RMSE), mean absolute error (MAE), mean bias error (MBE), correlation coefficient (R), and coefficient of determination (R^2) [6,14,15,21,24,34,39]. In the literature, applications considered successful typically report RMSE values in the range of 1–3 °C, MBE values close to zero, and R^2 values exceeding 0.70 [10,14,34,39,45,46,47]. Nevertheless, it has also been emphasized that model performance varies substantially depending on the spatial resolution of the satellite data used, the topographic and land-cover heterogeneity of the study area, and the type of model employed [2,7,38,46,48].

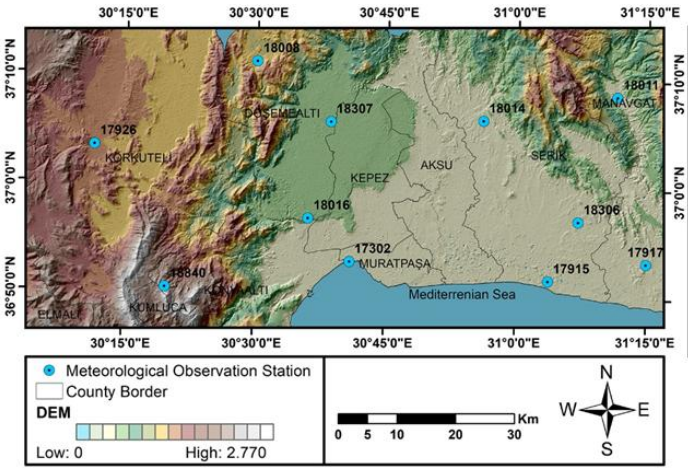
Accurate estimation of Ta-est is of critical importance, particularly in regions characterized by complex land-cover patterns and spatially sparse meteorological station networks, such as Mediterranean coastal cities. The study area, located in the Mediterranean climate zone, contains numerous microclimatic regions due to its complex land use structure, which combines coastal-mountainous topography, dense urban development, and agricultural areas [49,50,51], and this situation leads to sharp variations in air temperature over short distances. Owing to these characteristics, the study area not only allows the LST-Ta relationship to be examined at high spatial resolution and monthly scales but also possesses strong representativeness, enabling the derivation of results that can be generalized to similar regions within the Mediterranean climate zone. Due to the heterogeneous structure of the study area, station-based interpolation approaches and MODIS-based models with lower spatial resolution are unable to adequately represent microclimatic variability under heterogeneous surface conditions. To overcome these limitations, this study aims to estimate air temperature at the pixel scale by modeling high-spatial-resolution Landsat 8 data together with meteorological station measurements (Ta). By examining the

LST-Ta relationship at monthly scales under the complex and heterogeneous surface conditions of the Mediterranean climate zone, this study represents one of the limited number of investigations addressing the gap arising from the insufficient ability of low-resolution satellite- and station-based approaches to capture microclimatic variability. For this aim, LST data derived from high-spatial-resolution monthly Landsat 8 imagery for the 2016–2019 period and air temperature measurements obtained from 11 meteorological stations within the study area were used to develop linear, logarithmic, exponential, and second-order polynomial regression models to characterize the LST–Ta relationship. The performance of the developed regression models was evaluated in terms of statistical stability, temporal consistency, and generalizability using RMSE, MBE, and R^2 metrics, and the most suitable model for estimating Ta from satellite-based LST data was identified. Using the regression model that provided optimal performance, high-resolution monthly air temperature estimation (Ta-est) maps were generated from satellite-based LST data, and the agreement between these maps and temperature observations measured at meteorological stations was assessed using Pearson correlation analysis. The methodology and results of this study reveal the monthly performance of the LST-Ta relationship at high spatial resolution and provide both a methodological framework and reliable, generalizable data for microclimate modeling and planning studies in similar regions within the Mediterranean climate zone.

2. Materials and methods

2.1. Study area

The Antalya province is located in the Mediterranean Basin in southern Türkiye (36°53'12.28"N, 30°42'23.25"E). The province ranks fifth nationwide in population, attracts the largest number of tourists, and serves as a major producer of citrus fruits and greenhouse vegetables. Covering a surface area of 20,177 km², the province is predominantly mountainous (77.8%), with plains accounting for 10.2% and rough terrain for 12% of the total area (Figure 1) [52].



Station Number	Station Name	Altitude
17302	Antalya Region	47
17915	Serik/Belek	6
17917	Manavgat/Taşağıl	38
17926	Korkuteli	1017
18008	Dağbeli	789
18011	Manavgat/Beşkonak	142
18014	Serik/Gebiz	78
18016	Döşemealtı/Nebiler	266
18306	Serik	94
18307	Döşemealtı/Karain	308
18840	Saklıkent	1880

Figure 1: Map of the study area boundary in Antalya, Türkiye.

According to the Köppen–Geiger climate classification, Antalya is characterized by a Csa climate type [53]. Long-term climatic data indicate an annual mean temperature of 18.8 °C, reflecting the dominance of a mild to warm thermal regime throughout the year and confirming that the study area exhibits typical Mediterranean climate characteristics. While average monthly temperatures remain around 10 °C during the winter months, they exceed 28 °C in summer. In particular, the fact that

average maximum temperatures surpass 34 °C in July and August, and that the recorded absolute maximum temperature reaches 45.0 °C, indicates that extreme heat waves can be effective during the summer period. Moreover, the average minimum temperatures in winter months are around 6–8 °C, and the lowest recorded temperature is limited to −4.6 °C, indicating that frost events are rare and short-lived. Antalya experiences approximately 300 sunny days per year, with an annual average daily sunshine duration of 8.2 hours, increasing to 11–12 hours during the summer months (Table 1). The relatively high level of sunshine even in winter highlights the city's considerable potential in terms of energy production, agricultural activity, tourism, and outdoor space use. The annual total precipitation in Antalya amounts to 1053.4 mm, with rainfall largely concentrated in the winter season. December and January are the wettest months, whereas both precipitation amounts and the number of rainy days decrease markedly in July and August, during which dry conditions prevail. This pronounced seasonal distribution reflects the characteristic Mediterranean climate pattern of wet winters and hot, dry summers observed in Antalya [54].

Table 1: Long-term climatic parameters of the study area [54].

ANTALYA Measurement Period (1930 - 2023)	Months												Annual
	1.	2.	3.	4.	5.	6.	7.	8.	9.	10.	11.	12.	
Parameters													
Mean Monthly Temperature (°C)	**10.0**	**10.7**	**12.9**	**16.4**	**20.6**	**25.3**	**28.6**	**28.4**	**25.3**	**20.6**	**15.5**	**11.7**	**18.8**
Mean Maximum Temperature (°C)	**14.9**	**15.6**	**18.0**	**21.4**	**25.7**	**30.7**	**34.2**	**34.1**	**31.2**	**26.6**	**21.3**	**16.7**	**24.2**
Mean Minimum Temperature(°C)	**6.0**	**6.4**	**8.1**	**11.3**	**15.3**	**19.7**	**22.8**	**22.8**	**19.5**	**15.3**	**10.9**	**7.7**	**13.8**
Mean sunshine (hour)	**5.1**	**5.8**	**6.7**	**8.0**	**9.8**	**11.4**	**11.8**	**11.3**	**9.8**	**7.9**	**6.3**	**4.9**	**8.2**
Mean wet day number	**12.5**	**10.5**	**8.6**	**6.51**	**5.2**	**2.6**	**0.5**	**0.6**	**1.71**	**5.5**	**7.5**	**11.9**	**73.5**
Monthly rainfall (mm)	**234.5**	**150.2**	**92.1**	**49.0**	**34.3**	**11.0**	**4.4**	**4.3**	**16.9**	**70.9**	**129.7**	**256.**	**1053.4**
Record maximum temperature (°C)	**23.9**	**26.7**	**28.6**	**36.4**	**41.7**	**44.8**	**45.0**	**44.6**	**42.5**	**41.2**	**33.0**	**25.4**	**45**
Record minimum temperature (°C)	**-4.3**	**-4.6**	**-1.6**	**1.4**	**6.7**	**11.1**	**14.8**	**13.6**	**10.3**	**4.9**	**0.0**	**-1.9**	**-4.6**

2.2. Datasets

The study consists of two types of datasets. The first consists of LST data derived from Landsat 8 satellite imagery, while the second comprises in situ air temperature measurements from meteorological stations. Landsat 8 bands 4 (Red), 5 (NIR), and 10 (Thermal Infrared, resampled to 30 m) were freely obtained from the United States Geological Survey (USGS) Earth Explorer platform and used to retrieve LST [25]. Landsat 8 provides medium-to-high spatial resolution data ranging from 15 m to 100 m (Table 2). To minimize atmospheric interference, satellite images with no or minimal cloud cover were selected for each of the 12 months. In this study, minimal cloudiness was defined as less than 5% coverage. Accordingly, appropriate satellite and meteorological station datasets covering the period from 2016 to 2019 were employed. The acquisition time of the monthly satellite images was approximately consistent, ranging between 11:33 and 11:34 local time.

Table 2: Landsat 8 spectral bands used in the study [25].

Spectral Range	Wavelength (µm)	Resolution (m)
Band 4 – Red	0.64 - 0.67µm	30
Band 5 - Near-Infrared	0.85 - 0.88 µm	30
Band 10 - TIRS 1	10.6 - 11.19 µm	100 resampled to 30[a]
[a] Band 10 (TIRS) is acquired at 100 m, and Band 6's resolution is acquired at 100 m but has been resampled to 30 m in the delivered data product.		

Hourly air temperature data were obtained from 11 meteorological stations operated by the Turkish State Meteorological Service and located at elevations ranging from 6 m to 1880 m, on the dates when satellite images were acquired. The basis for selecting 11 meteorological stations is that usable temperature measurements were only available at these stations during the study period (2016-2019) [54]. Moreover, the satellite images for this region were captured at 11:33 and 11:34 local time. Therefore, the arithmetic averages of the air temperature (T_a) data from the meteorological stations at 11:00 and 12:00 local time were used for the estimation.

2.3. Methods

The study was conducted in four main stages: data collection, dataset preparation, analysis, and evaluation of the results (Figure 2). In the first stage, open-access Landsat 8 OLI/TIRS satellite images for each month and air temperature (Ta) data obtained from meteorological stations located in 11 different regions were acquired. Subsequently, the boundaries of the study area were delineated, and the locations of the meteorological stations within the study area were defined as point data in a GIS environment based on station coordinates. The necessary datasets for calculating land surface temperature (LST) were then generated. To ensure spatial consistency, all datasets were defined using the WGS84 / UTM Zone 36N datum and projection system.

The derivation of land surface temperature (LST) from Landsat 8 OLI/TIRS satellite imagery follows the single-channel method, which is widely used in the literature and consists of six main stages (Table 3) [55,56]. In the first stage, the digital number (DN) values of the thermal infrared band (Band 10) of the Landsat 8 OLI/TIRS imagery were converted into Top of Atmosphere (TOA) spectral radiance values using radiometric rescaling coefficients obtained from the satellite metadata file (Equation 1) [25,57]. In the second stage, TOA radiance values were transformed into sensor brightness temperature using the Landsat 8 OLI/TIRS-specific thermal calibration constants K1 and K2 (Equation 2). For Landsat 8 OLI/TIRS imagery, the K1 and K2 calibration constants are 774.89 and 1321.079, respectively. Since the calculated temperature values are obtained in Kelvin, they were converted to degrees Celsius by subtracting 273.15 [25,50,57]. In the third stage, a Normalized Difference Vegetation Index (NDVI) map was generated using the red (Band 4) and near-infrared (Band 5) bands of the Landsat 8 OLI/TIRS imagery (Equation 3). The NDVI, which ranges between −1 and +1, is a widely used indicator for quantitatively determining the spatial distribution and density of vegetation cover [56,58]. In the fourth stage, the proportion of vegetation cover (Pv) required for surface emissivity estimation was calculated according to the method proposed by Carlson and Ripley [59], taking into account the minimum and maximum NDVI values derived from the NDVI histogram (Equation 4) [50,56,60]. In the fifth stage, land surface emissivity (ε) was estimated as a function of vegetation proportion (Equation 5) [56,60]. Surface emissivity represents a surface's capacity to emit and absorb radiation within the longwave spectrum and varies according to land cover characteristics in the study area, including vegetation type and density, soil structure, and surface roughness [61,62]. In general, emissivity values increase with higher surface blackness and matte characteristics, whereas increased reflectivity leads to lower emissivity values [63]. In the sixth and final stage, atmospheric and emissivity corrections were

applied to the sensor-measured brightness temperature values to remove atmospheric effects, resulting in the generation of an LST map representing actual land surface temperature (Equation 6) [32,55,63].

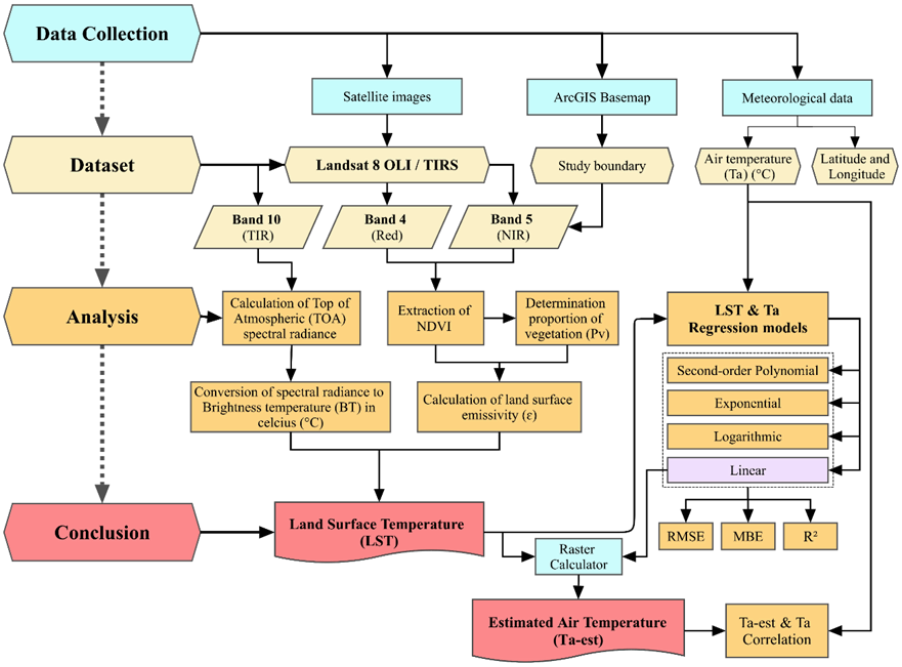


Figure 2: Flowchart of the study methodology.

Table 3: Equations used for deriving LST from Landsat 8 OLI/TIRS satellite imagery

Equations	Formulas	Descriptions
Equation 1:	$L_\lambda = M_L * Q_{cal} + A_L$	L_λ = TOA spectral radiance (Watts/ (m^2 * sr * µm)) M_L = Radiance multiplicative band A_L = Radiance add band Q_{cal} = Quantized and calibrated standard product pixel values
Equation 2:	$B_T = K_2 / ln(K_1 / (L_\lambda + 1)) - 273.15$	B_T = Top of atmosphere brightness temperature (°C) L_λ = TOA spectral radiance (Watts/(m^2 * sr * µm)) K_1 and K_2 = Band-specific thermal conversion constant from the metadata
Equation 3:	$NDVI = \rho NIR - \rho R / \rho NIR + \rho R$	$NDVI$ = Normalized difference vegetation index ρNIR = Near-Infrared band reflection (Band 5) ρR = Red band reflection (Band 4)
Equation 4:	$Pv = [NDVI - NDVI_{min} / NDVI_{max} - NDVI_{min}]^2$	Pv= Proportional vegetation $NDVI$ = Normalized difference vegetation index $NDVI_{max}$ = Maximum Normalized Difference Vegetation index $NDVI_{min}$ = Minimum Normalized Difference Vegetation index
Equation 5:	$\varepsilon = 0.004 * Pv + 0.986$	ε = Land surface emissivity Pv= Proportional vegetation
Equation 6:	$Ts = B_T / \{1 + [\lambda * B_T / \rho]. Ln\varepsilon\}$	B_T = Top of atmosphere brightness temperature (°C) λ = Wavelength of emitted radiance ε = Land Surface Emissivity ρ – (h x c/σ) = 1.438 x 10^{-2} = 14380mK

From the monthly LST maps obtained, station-based land surface temperature values were extracted using the pixel values corresponding to the locations of the meteorological stations. These values were jointly analyzed with the air temperature (Ta) data measured simultaneously by the same stations to develop regression models aimed at characterizing the LST-Ta relationship. The literature indicates that the

relationship between LST and Ta may deviate from linearity and exhibit nonlinear behavior depending on surface characteristics, vegetation density, atmospheric conditions, and seasonal variability [14,47,48,64]. For this reason, linear, logarithmic, exponential, and second-degree polynomial regression models representing different functional relationships were created within the scope of the study. The linear model was employed to represent the fundamental and direct relationship between LST and Ta [14,44], whereas the logarithmic and exponential models were used to capture potential saturation effects or accelerated changes within specific temperature ranges [34]. The second-order polynomial model was included to account for the curvilinear structure of the relationship and potential threshold behaviors [65]. The performance of the regression models developed to estimate air temperature from satellite-based land surface temperature data was evaluated and compared at both monthly and annual temporal scales using the Root Mean Square Error (RMSE), Mean Bias Error (MBE), and the coefficient of determination (R^2). While RMSE quantifies the magnitude of prediction errors, the MBE model systematically reveals whether there is a bias toward hot or cold. The R^2 value represents the explanatory power of LST in predicting Ta [10,14,34,39,45,46,47]. This multi-criteria evaluation framework enabled a simultaneous assessment of both the accuracy and explanatory capability of the models. Based on the results obtained, the regression model to be used in estimating air temperature from land surface temperature was determined by considering criteria such as generalizability, temporal consistency, and bias, in addition to error metrics. The model chosen for estimation was used as the research model in the subsequent analyses of the study. By applying this selected regression model to the monthly LST maps within a GIS software, spatially explicit air temperature estimation maps were generated from satellite-derived surface temperature data. To evaluate the level of agreement between the estimated air temperature values derived from these maps and the air temperature measurements recorded at meteorological stations, Pearson correlation analysis was conducted.

3. Results and Discussion

The results revealed a very strong correlation between air temperature (T_a) and LST, particularly in certain months. Monthly LST values and the corresponding air temperature (T_a) measurements from meteorological stations are presented in Figure 3. As shown, maximum and mean LST values exhibit trends similar to those of air temperature, while LSTmin closely matches Ta-min across most months, except in March and July. As expected, both LSTmax and LSTave follow slightly higher trends than the observed air temperature (T_a).

The performance indicators of the used regression models at annual and monthly scales (RMSE, MBE, and R^2) are presented in Table 4. At the annual scale, Table 4 shows that the linear model explains the LST–T_a relationship with high accuracy, yielding an R^2 value of 0.90, and demonstrates an acceptable error level with an RMSE of 2.71 °C. In particular, the MBE value of −0.00028 indicates that the linear model does not exhibit a pronounced overestimation or underestimation tendency in annual averages and produces statistically negligible bias, reflecting unbiased and reliable performance. Although the logarithmic model demonstrates a similar annual explanatory power (R^2 = 0.90) and neutrality (MBE = −0.00011), it does not provide a notable improvement over the linear model in terms of error magnitude (RMSE = 2.72 °C). In contrast, the exponential model exhibits a lower annual R^2 value (R^2 = 0.89), a higher error level (RMSE = 2.90 °C), and a pronounced negative MBE (−0.14), indicating a systematic cold bias. This suggests that, particularly under high-temperature conditions, the model tends to underestimate Ta, thereby limiting its generalizability. Although the second-order polynomial model yields the lowest annual error (RMSE = 2.52 °C) and the highest R^2 value (R^2 = 0.91), it fails to consistently maintain this performance at the monthly

scale. Moreover, the relatively higher level of systematic warm bias (MBE = 0.00806) compared to the linear and logarithmic models indicates that the model's generalizability remains constrained.

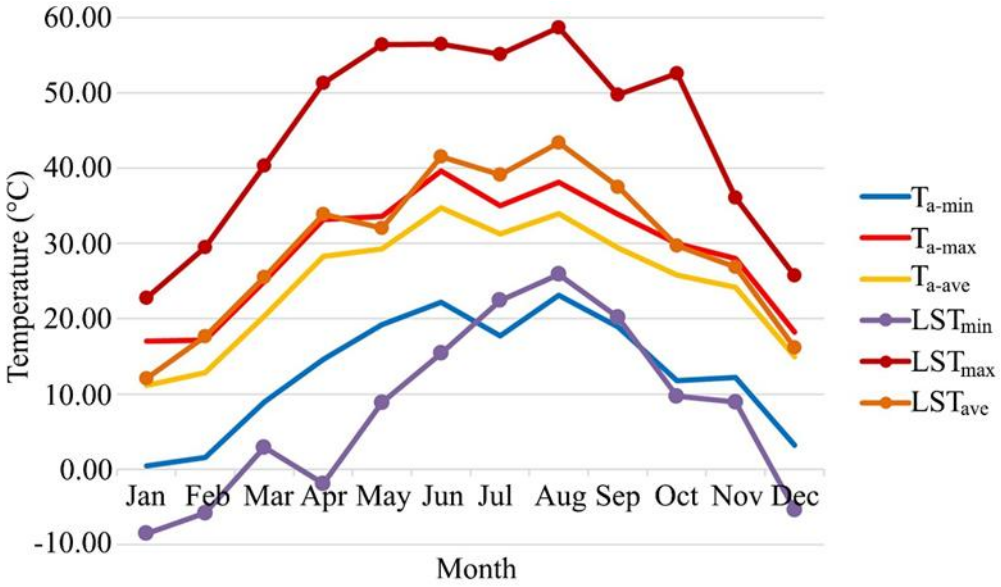


Figure 3: Comparison of LST and meteorology station temperature measurements (T_a).

Monthly analyses reveal that model performances exhibit pronounced seasonal variability. Examination of the monthly performance of the linear model indicates that it demonstrates a generally consistent, yet seasonally varying, level of accuracy throughout the year. During the winter months (December, January, and February), the model strongly explains the LST–Ta relationship, with high R^2 values ranging from 0.91 to 0.96 and low RMSE values between 0.87 and 1.39 °C. The MBE values remaining very close to zero (from −0.00064 to 0.00039) further indicate that the model does not exhibit a pronounced overestimation or underestimation tendency during this period. In the spring months (March–April), although a gradual decrease in explanatory power is observed (R^2 = 0.85–0.57), the relatively limited levels of error and bias indicate that the model maintains its stability. However, in May, model performance weakens (R^2 = 0.27), and RMSE values exceed 3 °C, which can be attributed to increasing heterogeneity in surface–atmosphere energy exchanges and the onset of the vegetation growth period. Nevertheless, the absence of a pronounced systematic bias suggests that the model retains a degree of adaptability even under these conditions. During the summer months (June–August), increased evapotranspiration and the strengthening influence of vegetation further complicate the heterogeneity of surface–atmosphere energy exchanges. Consequently, R^2 values decline, particularly in August (0.37–0.80), while RMSE values increase (2.20–2.91 °C). Despite this, MBE values remain close to zero, indicating that the linear model does not produce systematic bias even during this period. In the autumn months (September–November), although explanatory power decreases to its lowest levels (R^2 = 0.13–0.45), the balanced error and bias values suggest that the linear model provides a temporally consistent, non-overfitted, and generalizable performance across the annual cycle.

An evaluation of the monthly performance of the logarithmic model indicates that, similar to the linear model, it exhibits pronounced seasonality while demonstrating relatively higher explanatory power in certain months. During the winter period, particularly in December and February, the model performs at a high level. In February, the model achieves an R^2 value exceeding 0.95 and an RMSE below 0.80 °C, while in December it estimates the LST–Ta relationship with very high explanatory power (R^2 = 0.99) and a remarkably low error level (RMSE = 0.47 °C). The MBE values remaining

close to zero during these months indicate that the logarithmic model produces unbiased and stable estimates under cold-season conditions. In the spring months (March–May), although explanatory power gradually decreases (R^2 = 0.83, 0.58, and 0.28), the increase of RMSE values beyond 3 °C and a partial rise in warm bias suggest that the model retains a limited degree of adaptability. During the summer months (June–August), a pronounced deterioration in model performance is observed, with the R^2 value declining to 0.37 in August, while RMSE approaches approximately 3 °C. Moreover, the fluctuation of MBE values within restricted positive and negative ranges during this period indicates that the model produces more biased estimates compared to the linear model. In the autumn months (September–November), as explanatory power declines to its lowest levels (R^2 = 0.13–0.45) and error magnitudes remain comparable to those observed in summer, the logarithmic model demonstrates that, despite providing high accuracy in certain months, it fails to deliver a consistent and generalizable performance throughout the entire year.

Table 4. Performance metrics of regression models at annual and monthly scales

Season	Month	Linear			Logarithmic			Exponential			Second-order Polynomial		
		RMSE	MBE	R^2	RMSE	MBE	R^2	RMSE	MBE	R^2	RMSE	MBE	R^2
Winter	December	0,87	0,00039	0,96	0,47	0,00005	0,99	1,79	0,01607	0,86	0,42	0,00454	0,99
	January	1,39	-0,00064	0,91	2,26	0,00000	0,76	1,69	0,14530	0,89	1,14	0,00947	0,94
	February	0,95	-0,00028	0,93	0,80	0,00141	0,95	2,02	0,04465	0,78	0,78	-0,00283	0,96
Spring	March	1,53	-0,00067	0,85	1,64	0,00021	0,83	1,43	-0,07366	0,87	1,39	-0,01130	0,88
	April	3,36	-0,00133	0,57	3,32	-0,00190	0,58	3,56	-0,22324	0,53	2,99	0,02089	0,66
	May	3,45	-0,00131	0,27	3,43	0,00152	0,28	3,50	-0,19389	0,26	3,35	-0,03346	0,32
Summer	June	2,62	0,00153	0,68	2,54	-0,00485	0,70	2,80	-0,13140	0,64	2,11	0,06738	0,79
	July	2,20	0,00141	0,80	2,02	0,00488	0,83	2,66	-0,06283	0,73	1,31	0,05973	0,93
	August	2,91	-0,00194	0,37	2,91	-0,00097	0,37	2,92	-0,16664	0,37	2,91	0,03252	0,37
Autumn	September	3,26	0,00022	0,13	3,26	-0,00025	0,13	3,26	-0,21007	0,13	3,19	-0,05738	0,16
	October	4,33	-0,00104	0,29	4,31	-0,00064	0,30	4,47	-0,52050	0,27	4,22	0,03700	0,33
	November	3,05	0,00033	0,45	3,04	-0,00080	0,45	3,14	-0,30271	0,43	3,03	-0,02987	0,45
Annual		**2,71**	**-0,00028**	**0,90**	**2,72**	**-0,00011**	**0,90**	**2,90**	**-0,13991**	**0,89**	**2,52**	**0,00806**	**0,91**

An examination of the monthly performance of the exponential model indicates that, compared to the other models, it exhibits lower explanatory power and more pronounced bias throughout the year. Although model performance is relatively better during the winter months, particularly in December and January, its ability to estimate the LST–Ta relationship declines in February, with an R^2 value of 0.78 and an RMSE exceeding 2 °C. Moreover, the positive MBE values observed even during these months (notably 0.15 °C in January) indicate that the model tends to systematically overestimate air temperature. During the spring months (March–April), explanatory power decreases from 0.87 to 0.53, while RMSE values increase substantially from 1.43 °C to 3.56 °C and MBE shifts toward negative values, indicating a weakening of both accuracy and stability during this period. In May, model performance deteriorates further (R^2 = 0.26), with persistently high RMSE values and continued negative bias. Throughout the summer months (June–August), the decline in performance of the exponential model persists, with R^2 dropping to 0.37 in August and RMSE increasing to approximately 3 °C. The consistently negative MBE values with relatively large magnitudes during the summer period indicate that the model systematically underestimates Ta, particularly under high-

temperature conditions. A similar trend is observed in the autumn months (September–November), where R^2 values remain within the range of 0.13–0.43, and RMSE values exceed 3 °C. MBE values ranging from −0.21 to −0.52 further indicate a pronounced cold bias. Overall, the systematic bias and elevated error levels observed throughout the year demonstrate that the exponential model fails to provide a balanced and generalizable solution at the monthly scale.

An evaluation of the monthly performance of the second-order polynomial model indicates that, although the model provides very high explanatory power in certain months, it fails to maintain consistency throughout the year. During the winter months, the model exhibits strong performance and produces the best results among all models in terms of both explanatory power and error magnitude, particularly in February (R^2 = 0.96, RMSE = 0.78 °C) and December (R^2 = 0.99, RMSE = 0.42 °C). Similarly, in January, the model demonstrates high explanatory capability (R^2 = 0.94) and low error levels (RMSE = 1.14 °C). However, the tendency of MBE toward positive values during the winter months indicates that the model exhibits a slight warm bias. In the spring months (March–April), although explanatory power remains relatively high (R^2 = 0.88–0.66), the increase in RMSE values (RMSE = 1.40–2.99 °C) and the amplification of MBE in both positive and negative directions indicate that the model's sensitivity to increasing temperatures intensifies in a nonlinear manner. In May, a pronounced decline in explanatory power (R^2 = 0.32), RMSE values exceeding 3 °C, and an increase in negative bias collectively weaken the model's ability to estimate the LST–Ta relationship. During the summer months (June–August), model performance deteriorates markedly, with R^2 values declining to as low as 0.37 in August and RMSE values approaching approximately 3 °C. The emergence of positive and relatively high MBE values during this period, particularly in June and July, indicates that the model tends to systematically overestimate Ta under high-temperature conditions. In the autumn months (September–November), while explanatory power remains low (R^2 = 0.16–0.45), RMSE values remain around 3 °C and MBE shifts between positive and negative values, revealing increasing instability in model behavior. Overall, although the second-order polynomial model demonstrates superior performance in certain months, it fails to provide a stable and generalizable solution at the monthly scale.

During the winter months (January, February, and December), all models produce high R^2 values. In cold periods, the surface–atmosphere energy exchange tends to be more homogeneous, and thermal variability driven by evapotranspiration and vegetation activity remains limited. As a result, the relationship between LST and Ta largely exhibits a linear structure [14,34,47]. Lower solar elevation angles and weakened latent heat fluxes promote a more linear relationship between surface temperature and air temperature, thereby enhancing the explanatory power of linear regression models. Indeed, previous studies have demonstrated that the LST–Ta relationship is more stable and predictable during winter months compared to summer periods, and that linear models yield more reliable results under such conditions [14,15,34]. In contrast, a pronounced decline in model performance is observed during the summer and transitional seasons (particularly from May to October). During this period, increased evapotranspiration, surface moisture, vegetation activity, and anthropogenic heat emissions render the LST–Ta relationship more complex and nonlinear [5,14,15]. Although logarithmic and exponential models are theoretically designed to represent such nonlinear processes, they fail to produce more stable or lower-error results than the linear model at the monthly scale. This finding indicates that increasing model complexity does not necessarily confer advantages in terms of generalizability [34,66]. Similarly, the literature reports that nonlinear models may generate pronounced biases under high-temperature conditions and during periods dominated by strong latent heat fluxes, thereby limiting their generalizability [2,48]. Although the second-order polynomial model produces very high R^2 values and low error levels in certain months (e.g., February and December), it exhibits abrupt performance

declines, irregular error distributions, and pronounced systematic biases in other months. This behavior suggests that the model may be prone to overfitting within specific temperature ranges. Moreover, the magnitude of the performance improvement achieved during months of high model accuracy is relatively limited and remains within the ±1–2 °C uncertainty range of satellite-based surface temperature data reported in the literature [15,34,67]. Consistent with these findings, previous studies emphasize that although polynomial and other nonlinear regression models may yield high R^2 values in monthly or seasonal analyses with limited sample sizes, their generalizability to independent datasets and different temporal periods may be weak [2,14,15,65,68].

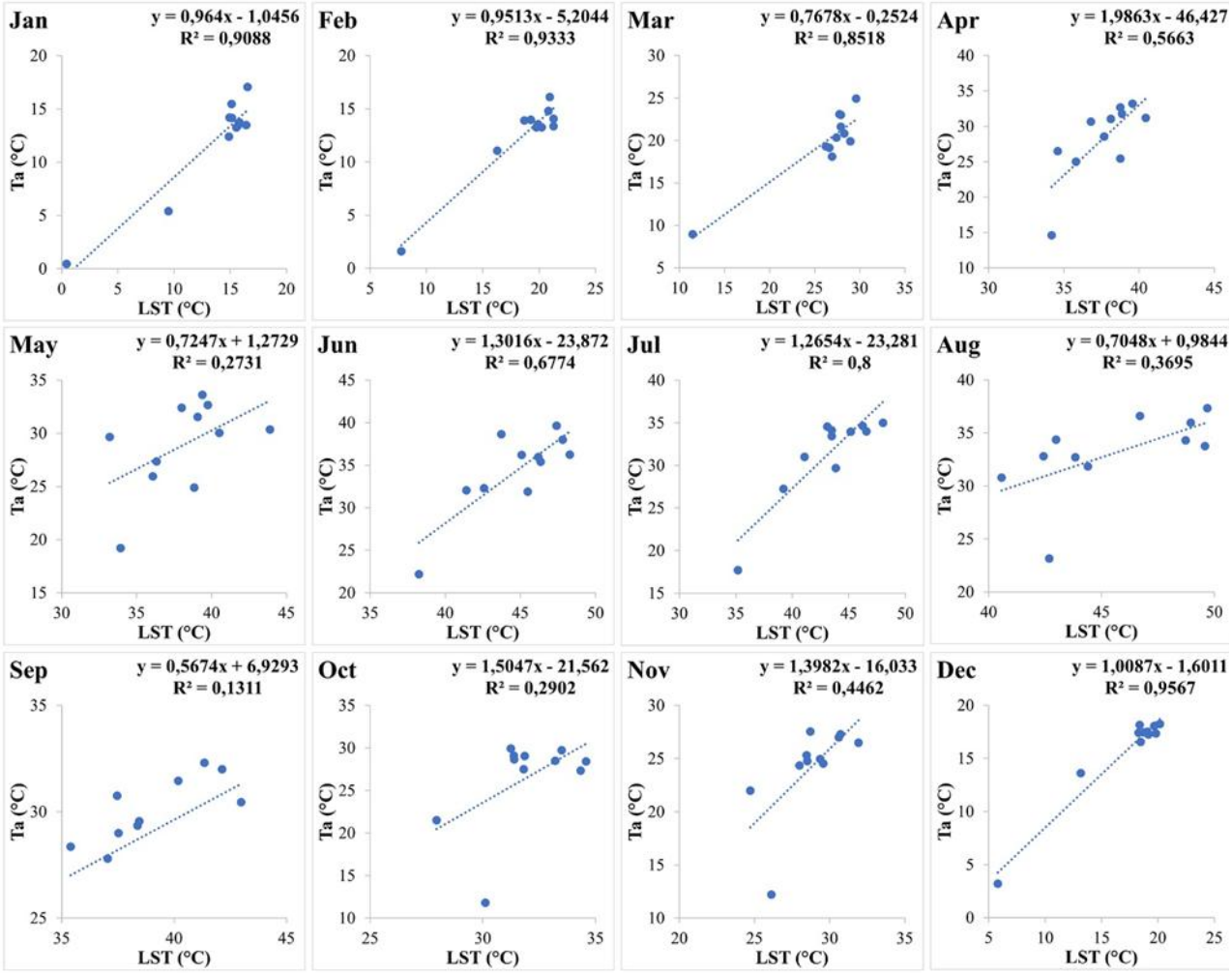


Figure 4: Monthly linear regression fits between Landsat 8-derived LST and air temperatures measured at meteorological stations for all stations. These regressions were used to estimate pixel-scale air temperatures from LST.

When the regression models developed within the scope of the study are compared, their performances at both monthly and annual scales (RMSE, MBE, and R^2) are evaluated jointly with measures of temporal consistency. This multi-criteria assessment reveals that the linear model produces more balanced, consistent, unbiased, and generalizable results across both monthly and annual scales compared to the other models. The linear model does not merely exhibit high performance during specific periods; rather, it stands out by maintaining low and stable error values throughout the year, bias levels close to zero, sustained low bias despite seasonal variability, and continuous explanatory power over time. In contrast, although the other nonlinear models achieve higher R^2 values in certain months, these gains are accompanied by higher error magnitudes or

pronounced systematic biases and cannot be consistently sustained at the monthly scale. The stable behavior exhibited by the linear model under varying seasonal conditions and despite fluctuations in surface–atmosphere energy exchanges indicates that the model provides a more robust and generalizable solution from both statistical and physical perspectives. For these reasons, the linear model was selected as the predictive model for estimating air temperature from satellite-based surface temperature data, and all subsequent analyses in the study were conducted using this model. The fitted relationships derived from the linear regression model are presented in Figure 4.

The maps showing the distribution of LST and estimated air temperature ($T_{a\text{-}est}$) over the months are given in Figures 5 and 6. It is seen from the distribution maps that LST and $T_{a\text{-}est}$ exhibit similar spatial distribution, and as expected, the LST ranges are higher than those of $T_{a\text{-}est}$. There is a correlation between the distributions of the two parameters.

Pearson correlation analysis was applied to determine the direction and degree of agreement between the air temperatures produced from the LST and the air temperatures measured. Figure 7 shows the correlation coefficients between the air temperature data obtained from LST and the air temperature data obtained from the meteorological station. Accordingly, the correlation coefficients show a rapid decrease from January to May and reach their lowest value in May. This result is probably an effect of the seasonal transition from winter to summer. The observation of a similar situation in September supports our opinion that our model works quite well in summer and winter, but its performance declines in spring and autumn. It peaks again at 0.90 in June and shows a downward trend again until September. From September onwards, it shows an upward trend and completes a one-year period.

The derived regression equations were implemented on the LST data using GIS software, and air temperature maps were generated at a spatial resolution of 30 m to achieve high estimation accuracy. The coherence among Ta-est, LST, and observed Ta was evaluated using Pearson correlation analysis. Strong correlations were identified for January, February, March, June, July, and December, whereas moderate correlations were observed for April, August, September, October, and November. In contrast, no statistically significant relationship was detected in May, indicating that Ta-est does not consistently represent the observed Ta during this period.

Table 5 presents the measured and estimated air temperatures ($T_{a\text{-}est}$). It is seen from the table that Ta-est in January, February, March, June, July, and December are in standard deviation ranges, while those belonging to April, August, September, and November are out of the standard deviation for only the Saklıkent Meteorology Station. In addition, the Ta-est values for May deviate from the standard deviation only at the Manavgat/Beşkonak and Saklıkent meteorological stations. When Ta-est at all the meteorological stations are evaluated cumulatively, 95% of the EATs are seen to be within the standard deviation ranges. It can be stated that Ta-est and measured air temperatures (T_a) show a close agreement, and the difference between them is mostly below 1°C. The biggest difference between $T_{a\text{-}est}$ and measured T_a is observed at Saklıkent station, which may be attributed to the station's specific location.

A significant relationship was found between measured air temperature (T_a) and LST for all stations, and 95% of the $T_{a\text{-}est}$ are within standard deviation ranges. Similar results with this study, which show close agreements between $T_{a\text{-}est}$ and T_a, are given in the literature [14,27]. The average difference between $T_{a\text{-}est}$ and T_a is 1.3°C, with the largest difference being 11.2°C. $T_{a\text{-}est}$ for the Saklıkent station gives the largest difference in the standard deviation, possibly due to its altitude (1880 m), sunshine duration, the effect of snow cover, and cloud cover [69]. Topographic elevation is known to influence climate variables [70], and high-altitude regions are more sensitive and variable to air temperature (T_a) and climate change than other land surfaces at the same latitudes [71,72].

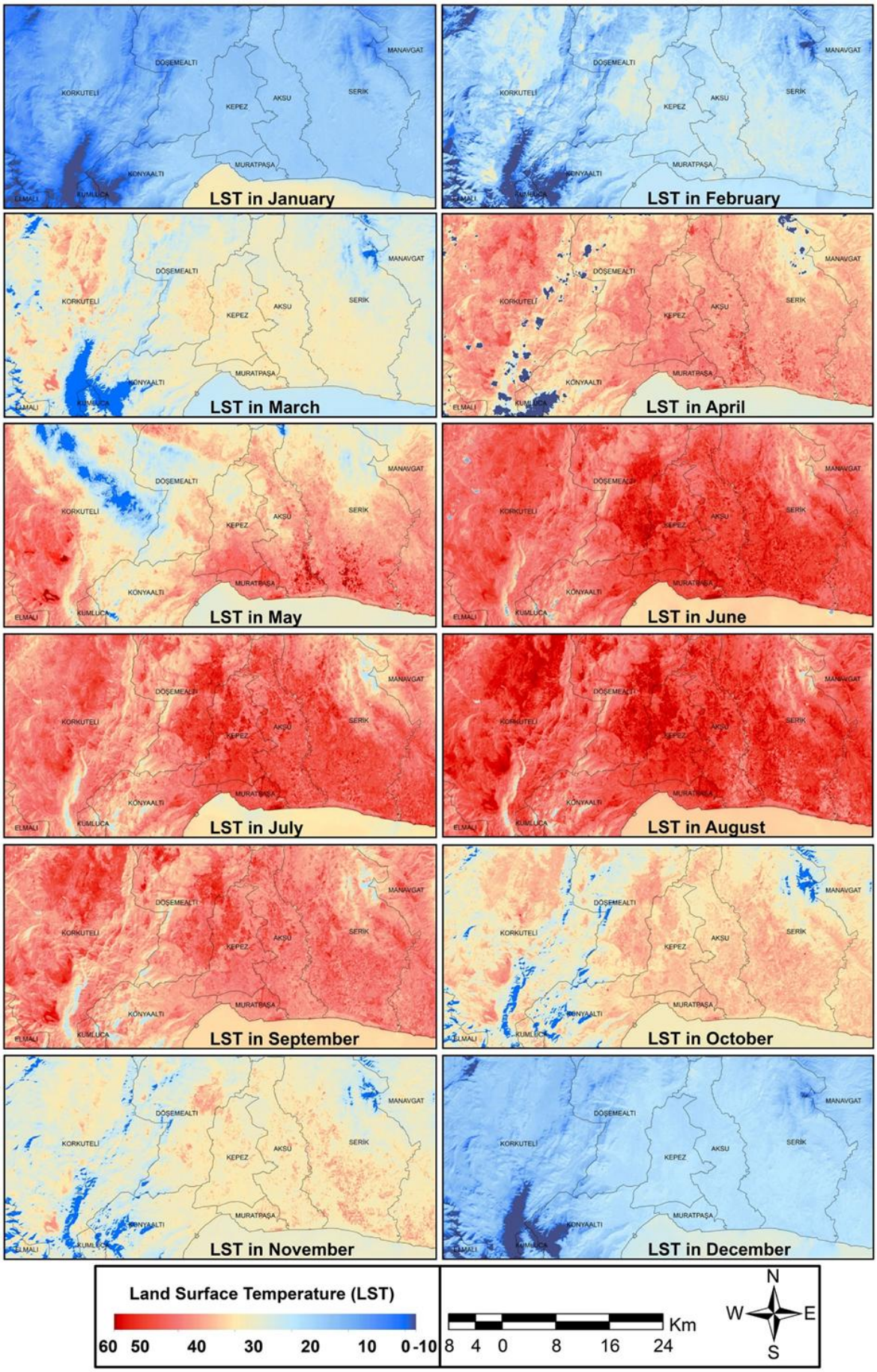


Figure 5: Land Surface Temperature (LST) maps.

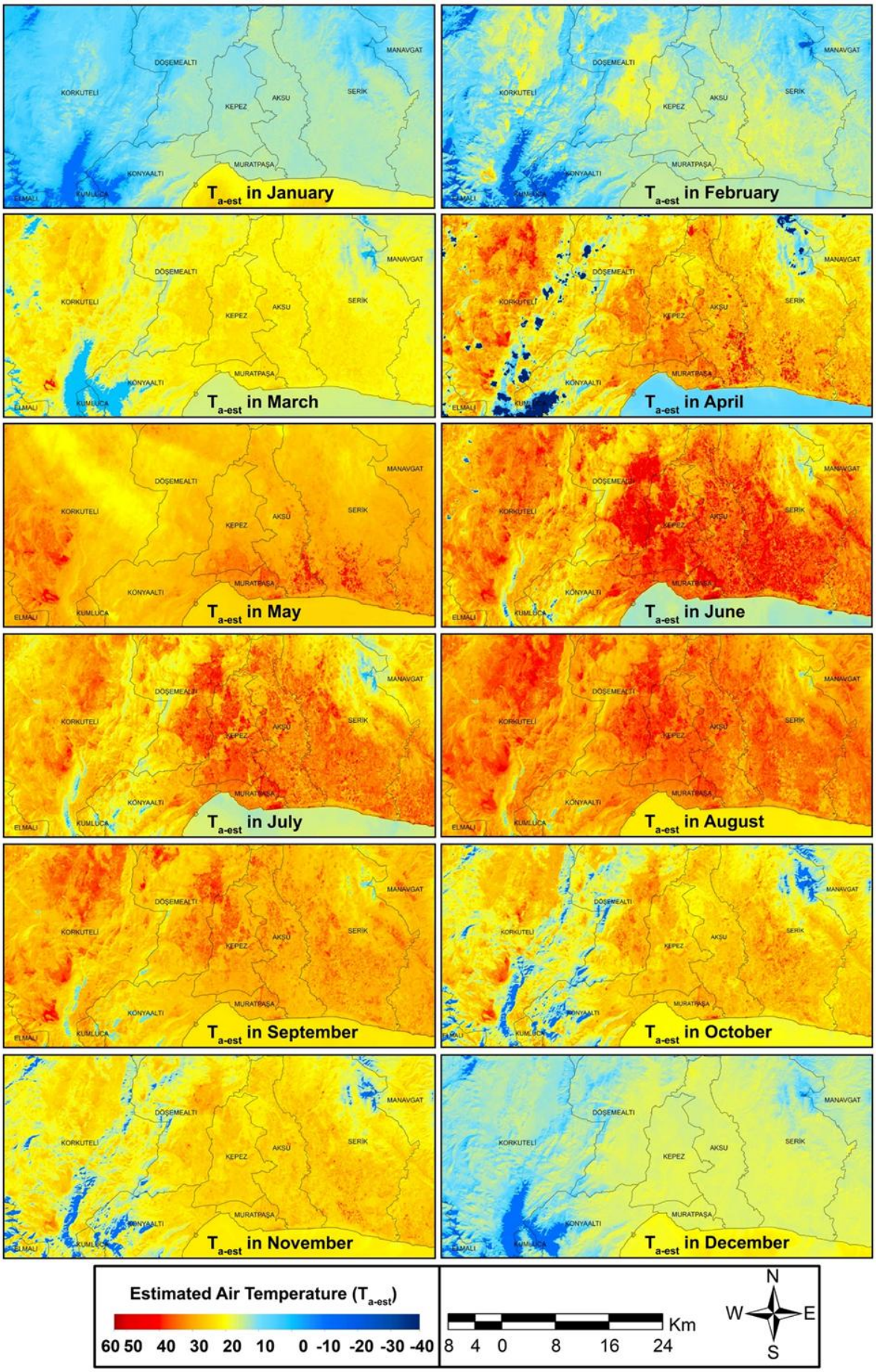


Figure 6: Estimated Air Temperature (Ta-est) maps.

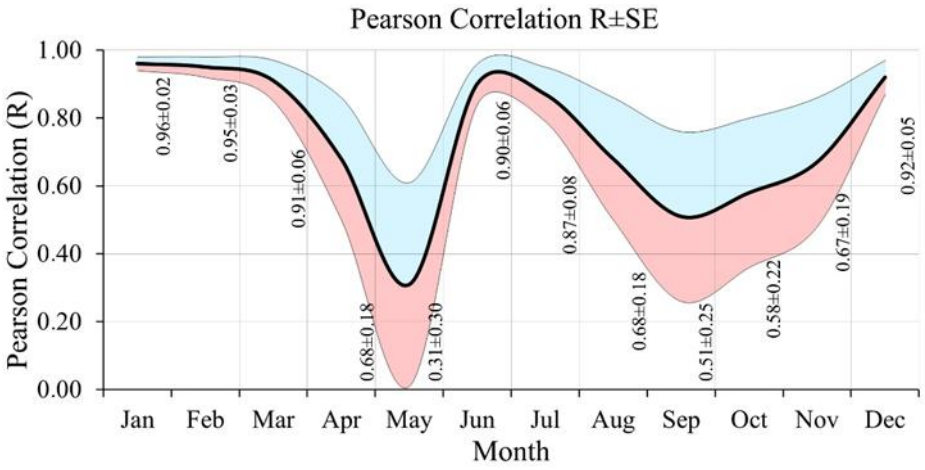


Figure 7. Calculated Pearson correlation coefficients and their standard errors.

Table 5: The air temperature measured by the meteorological station and the air temperature estimated from the LST.

Meteorology Station		Air Temperature (T_a) Measured by Meteorological Station & Estimated Air Temperature ($T_{a\text{-}est}$) (°C)												
No	Name		Jan	Feb	Mar	Apr	May	Jun	Jul	Aug	Sep	Oct	Nov	Dec
17302	Antalya Region	T_a	17.05	13.95	19.3	26.5	25.95	32.3	31	30.8	28.35	30	24.35	18.05
		$T_{a\text{-}est}$	14.56	13.23	20.24	24.67	29.46	31.62	29.61	29.03	25.74	24.73	23.49	17.8
		DIFF	2.49	0.72	-0.94	1.83	-3.51	0.68	1.39	1.77	2.61	5.27	0.86	0.25
17915	Serik/Belek	T_a	13.75	13.25	20.35	28.55	30.05	36.2	34.55	32.7	29.55	29.1	24.75	17.4
		$T_{a\text{-}est}$	13.87	13.68	21.17	30.04	30.66	35.39	32.06	31.92	28.28	25.7	24.18	16.51
		DIFF	-0.12	-0.43	-0.82	-1.49	-0.61	0.81	2.49	0.78	1.27	3.4	0.57	0.89
17917	Manavgat/Tasağıl	T_a	13.5	13.35	21.6	31.05	31.55	35.4	35	33.75	30.45	28.4	26.5	18.25
		$T_{a\text{-}est}$	14.44	15.17	21.56	30.82	30.27	37.28	38	37	32.03	29.92	28.57	18.25
		DIFF	-0.94	-1.82	0.04	0.23	1.28	-1.88	-3	-3.25	-1.58	-1.52	-2.07	0
17926	Korkuteli	T_a	5.4	11.05	18.1	25	27.35	32.05	27.25	32.8	27.8	21.5	22	13.6
		$T_{a\text{-}est}$	7.93	10.37	20.76	26.79	29.53	29.84	27.34	30.67	27.1	19.62	19.27	11.73
		DIFF	-2.53	0.68	-2.66	-1.79	-2.18	2.21	-0.09	2.13	0.7	1.88	2.73	1.87
18008	Dağbeli	T_a	7.8	13.15	19.35	26.8	27.95	33.9	29.65	34.55	29	23.8	22.65	13.05
		$T_{a\text{-}est}$	7.5	11.97	20.7	22.76	26.35	34.86	28.83	34.71	29.49	23.12	20.33	11.39
		DIFF	0.3	1.18	-1.35	4.04	1.6	-0.96	0.82	-0.16	-0.49	0.68	2.32	1.66
18011	Manavgat/Beşpınar	T_a	13.2	17.15	24.8	31.55	33.35	38.9	33.1	38.15	33.9	27.4	28	17.7
		$T_{a\text{-}est}$	12.7	15.14	21.14	26.38	29.13	34.43	28.57	34.2	30.9	26.2	25	15.94
		DIFF	0.5	2.01	3.66	5.17	4.22	4.47	4.53	3.95	3	1.2	3	1.76
18014	Serik/Gebiz	T_a	14.15	16.1	24.95	33.2	33.6	39.65	34.65	37.35	32.3	29.8	27	17.5
		$T_{a\text{-}est}$	13.26	14.86	22.88	33.31	30.36	38.89	35.84	37.09	30.68	28.24	26.88	17.23
		DIFF	0.89	1.24	2.07	-0.11	3.24	0.76	-1.19	0.26	1.62	1.56	0.12	0.27
1	Dö	T_a	12.4	13.25	20.8	30.65	29.65	35.95	33.45	36.6	29.35	27.5	24.95	16.55

Meteorology Station		**Air Temperature (T_a) Measured by Meteorological Station & Estimated Air Temperature ($T_{a\text{-}est}$) (°C)**											
No	**Name**		**Jan**	**Feb**	**Mar**	**Apr**	**May**	**Jun**	**Jul**	**Aug**	**Sep**	**Oct**	**Nov**	**Dec**
		$T_{a\text{-}est}$	12.99	14.16	21.83	28.51	28.69	37.05	32.54	34.45	28.21	25.61	25.29	16.66
		DIFF	-0.59	-0.91	-1.03	2.14	0.96	-1.1	0.91	2.15	1.14	1.89	-0.34	-0.11
18306	Serik	**T_a**	13.25	14.05	23	31.75	32.65	38	33.95	35.95	32	27.4	27.3	17.35
		$T_{a\text{-}est}$	13.61	15.16	21.56	32.09	30.46	39.52	34.55	36.44	31.33	29.53	27.03	17.92
		DIFF	-0.36	-1.11	1.44	-0.34	2.19	-1.52	-0.6	-0.49	0.67	-2.13	0.27	-0.57
18307	Döşemealtı/ Karain	**T_a**	11.55	14.65	22.6	31.05	30.45	37.6	33.6	37.75	31.75	26.75	26.5	12.35
		$T_{a\text{-}est}$	12.23	15.61	23.34	31.36	27.97	38.23	34.07	37.12	31.21	27.57	25.11	16.7
		DIFF	-0.68	-0.96	-0.74	-0.31	2.48	-0.63	-0.47	0.63	0.54	-0.82	1.39	-4.35
18840	Saklıkent	**T_a**	0.45	1.6	8.95	14.6	19.2	22.2	17.7	23.15	18.95	11.8	12.2	3.2
		$T_{a\text{-}est}$	-0.58	2.19	8.61	23.97	28.88	25.05	22.48	30.9	28.42	23	21.08	4.88
		DIFF	1.03	-0.59	0.34	-9.37	-9.68	-2.85	-4.78	-7.75	-9.47	-11.2	-8.88	-1.68
Std Dev.			4.75	4.07	4.38	5.21	4.15	4.85	5.10	4.30	3.94	5.27	4.41	4.75

In the study area, temperature differences increase with altitude up to 1000 m above sea level [73], while they decrease above this elevation. Most of the study area lies below 1000 m, where the 'Marine Mediterranean thermal regime,' characterized by hot summers and temperate winters, predominates [74]. However, with an altitude of 1800 m in Saklıkent, the high temperatures along the Mediterranean coast have changed due to the altitude and show the characteristics of a terrestrial transition-type thermal regime [75]. The direct or indirect relationship between location and environmental land uses and local temperatures [13,76] and warm temperature anomalies are factors explaining the difference in standard deviation at the Saklıkent station [77]. Since the other stations in the study area have similar environmental conditions, the air temperature maps produced from the surface temperature were in good agreement with the measurements of the meteorological stations.

Additionally, the temperature differences between the coldest and hottest months vary depending on the elevation of the meteorological stations [78] and seasonal changes [1]. The average air temperatures ($T_{a\text{-}ave}$) recorded at 11 meteorological stations showed a continuous increase from January to July, except for May, due to changes in cloud cover and sunshine duration [79,80]. Considering that LST derived from low-resolution satellite data may introduce errors and limitations in estimating air temperature ($T_{a\text{-}est}$) [44], the present study employed higher-resolution satellite imagery to improve estimation accuracy.

The large deviations observed at the Saklıkent station, located at the highest elevation within the study area, highlight the limitations of representing LST–air temperature relationships using simple linear models in high-altitude and topographically complex regions [7,8]. Variability in the near-surface vertical temperature gradient, driven by non-stationary elevation–temperature relationships, directly affects the accuracy of air temperature estimation models [7,69,17,73,78]. In addition, high albedo associated with snow cover and enhanced longwave radiation emission can increase the discrepancy between LST and air temperature [48,55,69]. These effects contribute to a weakening of the LST–Ta relationship, particularly in high-elevation areas, and increase model uncertainty associated with surface emissivity and atmospheric correction processes [8,33,47,58]. When these factors are considered collectively, the need emerges to develop elevation-adjusted regression models that are

compatible with elevation and other environmental variables, rather than relying on uniform linear regression models, especially in high-altitude microclimatic regions [8,21]. By explicitly incorporating lapse rate variability, snow cover effects, and high-altitude atmospheric characteristics into the modeling framework, both the generalizability and predictive capability of air temperature estimation models can be enhanced [7,66]. This approach enables the production of more robust estimates based not only on station data but also on parametric models that are sensitive to topographic and surface conditions, thereby systematically reducing elevation-related biases [8,45].

4. Conclusions

This study demonstrates that near-surface air temperature (Ta) within the specific context of Antalya Province and the Mediterranean (Csa) climate zone can be reliably estimated using LST data derived from Landsat 8 satellite imagery provided by the USGS at a spatial resolution of 30 m, and that the performances of the developed linear, logarithmic, exponential, and second-order polynomial regression models vary across temporal and seasonal scales. Although nonlinear models exhibit higher explanatory power in certain months, the fact that these gains are accompanied by higher error magnitudes and pronounced systematic biases limits their generalizability at the monthly scale. In contrast, the linear regression model emerges as the most reliable approach for estimating air temperature from satellite-based LST data for the study area, due to its stable performance throughout the year, low error levels, and negligible deviation, in terms of statistical stability, temporal consistency, and generalizability.

The results further indicate that the linear regression model estimates air temperature (T_a) from LST data with the highest accuracy during the winter months, when surface–atmosphere energy exchange is more homogeneous, whereas model performance weakens during the summer months, particularly in August, due to increased heterogeneity in energy exchange processes and the strengthening influence of vegetation. Similar declines in model performance are also observed during transitional periods, such as late spring (May) and early autumn (September–October). When air temperatures estimated from LST data using the linear regression model are compared with station-based observations, the absolute differences between estimated and observed values are found to be predominantly below 1 °C. These low error values and high accuracy have enabled the production of more detailed and reliable air temperature maps at a spatial resolution of 30 m in the study area characterized by the Csa climate type using Landsat 8 data, compared to MODIS-based studies with a spatial resolution of 1 km that are commonly used in the literature.

In conclusion, despite pronounced microclimatic variability over short distances caused by land cover and topographic heterogeneity, and despite seasonal variability in surface–atmosphere energy exchanges, the results demonstrate that for Mediterranean regions with similar climatic and topographic characteristics, high-resolution air temperature (Ta) maps can be effectively derived from satellite-based LST data using a linear regression approach. The findings and results of this study are expected to make significant contributions to the development of data-driven decision-support systems for environmental planning, agricultural management, disaster risk management, and the tourism sector, particularly in Mediterranean climate regions where microclimates are pronounced, and to provide a methodological foundation for future research. The limited temporal resolution of Landsat 8 and its sensitivity to cloud cover, lapse rate differences in high-elevation areas, the influence of snow cover on surface emissivity, and uncertainties associated with atmospheric correction methods may lead to local variability in model performance. Therefore, future studies

should focus on developing elevation-adjusted regression models and conducting comparative analyses through multi-sensor data integration and machine learning–based approaches (e.g., RF, ANN, and SVM), which would contribute substantially to improving both the accuracy and generalizability of air temperature (Ta) estimates derived from satellite-based LST data. In addition, the use of long-term time series encompassing seasonal and diurnal variability would enable a more detailed understanding of microclimatic variability and facilitate integration with climate models.

Author Contributions: Conceptualization, N.K. and S.S.; methodology, N.K., B.D. and A.K.; software, N.K., S.S. and R.O.; validation, N.K., S.S., A.K. and R.O.; formal analysis, N.K., B.D. and A.K.; investigation, N.K., S.S. and R.O.; resources, N.K., M.A. and E.K.; data curation, N.K., A.K. and R.O.; writing-original draft preparation, N.K., S.S., B.D., A.K. and R.O.; writing-review and editing, N.K., S.S., B.D., A.K., R.O., M.A. and E.K.; visualization, N.K. and R.O.; supervision, N.K. All authors have read and agreed to the published version of the manuscript.

Funding: This research received no external funding.

Data Availability Statement: The raw data supporting the conclusions of this article will be made available by the authors on request.

Conflicts of Interest: The authors declare no conflicts of interest.

Acknowledgments: We are also thankful to the anonymous reviewers for their insightful comments, which helped improve this paper. The authors have reviewed and edited the output and take full responsibility for the content of this publication.

Abbreviations: The following abbreviations are used in this manuscript.

LST	Land Surface Temperature
Ta	Air temperature
Ta-est	Estimated near-surface air temperature
TIR	Thermal Infrared
GIS	Geographic Information System
USGS	United States Geological Survey
RMSE	Root Mean Square Error
MAE	Mean Absolute Error
SE	Standard Error

References

[1] M. T. Burrows, D. S. Schoeman, L. B. Buckley, P. Moore, E. S. Poloczanska, K. M. Brander, et al., "The Pace of Shifting Climate in Marine and Terrestrial Ecosystems," *Science*, vol. 334, no. 6056, pp. 652-655, 2011, doi: 10.1126/science.1210288.

[2] T. Sun, R. Sun and L. Chen, "The Trend Inconsistency Between Land Surface Temperature and Near Surface Air Temperature in Assessing Urban Heat Island Effects," *Remote Sensing*, vol. 12, no. 8, 1271, 2020, doi: 10.3390/rs12081271.

[3] C. P. Morice, J. J. Kennedy, N. A. Rayner, J. P. Winn, E. Hogan, R. E. Killick, R. J. H. Dunn, T. J. Osborn, P. D. Jones and I. R. Simpson, "An Updated Assessment of Near-Surface Temperature Change From 1850: The Hadcrut5 Data Set," *J. Geophys. Res.*, vol. 126, no. 3, e2019JD032361, 2021, doi: 10.1029/2019JD032361

[4] M. Huang, S. Piao, P. Ciais, J. Peñuelas, X. Wang, T. F. Keenan, et al., "Air Temperature Optima of Vegetation Productivity Across Global Biomes," Nat. Ecol. Evol., vol. 3, no. 5, pp. 772-779, 2019, doi: 10.1038/s41559-019-0838-x.

[5] Q. Weng, "Thermal Infrared Remote Sensing for Urban Climate and Environmental Studies: Methods, Applications, and Trends," *ISPRS J. Photogramm. Remote Sens.*, vol. 64, no. 4, pp. 335-344, 2009, doi: 10.1016/j.isprsjprs.2009.03.007.

[6] H. Yan, J. Zhang, Y. Hou and Y. He, "Estimation of Air Temperature From Modis Data in East China," *Int. J. Remote Sens.*, vol. 30, no. 23, pp. 6261-6275, 2009, doi: 10.1080/01431160902842375.

[7] Z. Pan, J. Zhu, J. Liu, J. Gu, Z. Liu, F. Qin and Y. Pan, "Estimation of Air Temperature and the Mountain-Mass Effect in the Yellow River Basin Using Multi-Source Data," *Plos One*, vol. *16*, no. 10, e0258549, 2021, doi: 10.1371/journal.pone.0258549.
[8] T. R. Lookingbill and D. L. Urban, "Spatial Estimation of Air Temperature Differences for Landscape-Scale Studies in Montane Environments," *Agric. For. Meteorol.*, vol. 114, no. 3-4, pp. 141-151, 2003, doi: 10.1016/S0168-1923(02)00196-X.
[9] C. D. Ziter, E. J. Pedersen, C. J. Kucharik and M. G. Turner, "Scale-Dependent Interactions Between Tree Canopy Cover and Impervious Surfaces Reduce Daytime Urban Heat During Summer," *Proc. Natl. Acad. Sci.*, vol. 116, no. 15, pp. 7575-7580, 2019, doi: 10.1073/pnas.1817561116.
[10] G. Fu, Z. Shen, X. Zhang, P. Shi, Y. Zhang and J. Wu, "Estimating Air Temperature of an Alpine Meadow on the Northern Tibetan Plateau Using Modis Land Surface Temperature," *Acta Ecol. Sin.*, vol. 31, no. 1, pp. 8-13, 2011, doi: 10.1016/j.chnaes.2010.11.002.
[11] WMO. Available online: https://wmo.int/ (accessed on 5 January 2026).
[12] T. R. Oke, 2006. Initial guidance to obtain representative meteorological observations at urban sites, instruments and observing methods report no. 81. World Meteorological Organization. Available online: https://urban-climate.org/wp-content/uploads/2023/10/Oke_2006_IOM-81-UrbanMetObs.pdf (accessed on 12 March 2025).
[13] E. Krüger and B. Givoni, "Outdoor Measurements and Temperature Comparisons of Seven Monitoring Stations: Preliminary Studies in Curitiba, Brazil," *Built Environ.*, vol. 42, no. 4, pp. 1685-1698, 2007, doi: 10.1016/j.buildenv.2006.02.019.
[14] C. Vancutsem, P. Ceccato, T. Dinku and S. J. Connor, "Evaluation of Modis Land Surface Temperature Data to Estimate Air Temperature in Different Ecosystems Over Africa," *Remote Sens. Environ.*, vol. 114, no. 2, pp. 449-465, 2010, doi: 10.1016/j.rse.2009.10.002.
[15] N. Janatian, M. Sadeghi, S. H. Sanaeinejad, E. Bakhshian, A. Farid, S. M. Hasheminia, and S. Ghazanfari, "A Statistical Framework for Estimating Air Temperature Using Modis Land Surface Temperature Data," *Int. J. Climatol.*, vol. 37, no. 3, pp. 1181-1194, 2017, doi: 10.1002/joc.4766
[16] S. Li, D. A. Griffith and H. Shu, "Temperature Prediction Based on a Space-Time Regression-Kriging Model," *J. Appl. Stat.*, vol. 47, no. 7, pp. 1168-1190, 2020, doi: 10.1080/02664763.2019.1671962.
[17] A. Sekulić, M. Kilibarda, D. Protić, M. P. Tadić and B. Bajat, "Spatio-Temporal Regression Kriging Model of Mean Daily Temperature for Croatia. *Theor. Appl. Climatol.*, vol. 140, pp. 101-114, 2020, doi: 10.1007/s00704-019-03077-3.
[18] A. Shtiliyanova, G. Bellocchi, D. Borras, U. Eza, R. Martin and P. Carrère, "Kriging-Based Approach to Predict Missing Air Temperature Data," *Comput. Electron. Agr.*, vol. 142, pp. 440-449, 2017, doi: 10.1016/j.compag.2017.09.033.
[19] D. Cho, C. Yoo, J. Im, Y. Lee and J. Lee, "Improvement of Spatial Interpolation Accuracy of Daily Maximum Air Temperature in Urban Areas Using a Stacking Ensemble Technique," *GISci. Remote Sens.*, vol. 57, no. 5, pp. 633-649, 2020, doi: 10.1080/15481603.2020.1766768.
[20] Y. Rao, S. Liang, D. Wang, Y. Yu, Z. Song, Y. Zhou, M. Shen and B. Xu, "Estimating Daily Average Surface Air Temperature Using Satellite Land Surface Temperature and Top-of-Atmosphere Radiation Products Over the Tibetan Plateau," Remote Sens. Environ., vol. 234, 111462, 2019, doi: 10.1016/j.rse.2019.111462.
[21] Y. Xu, Z. Qin and Y. Shen, "Study on The Estimation of Near-Surface Air Temperature From Modis Data By Statistical Methods," Int. J. Remote Sens., vol. 33, no. 24, pp. 7629-7643, 2012, doi: 10.1080/01431161.2012.701351
[22] R. A. Muller, J. Wurtele, R. Rohde, R. Jacobsen, S. Perlmutter, A. Rosenfeld, J. Curry, D. Groom, C. Wickham and S. Mosher, "Earth Atmospheric Land Surface Temperature and Station Quality in the Contiguous United States," Geoinfor. Geostat.: An Overview, vol. 1, no.3, pp. 1-6, 2013, doi: 10.4172/2327-4581.1000107
[23] M. Otgonbayar, C. Atzberger, M. Mattiuzzi and A. Erdenedalai, "Estimation of Climatologies of Average Monthly Air Temperature Over Mongolia Using Modis Land Surface Temperature (LST) Time Series and Machine Learning Techniques," Remote Sensing, vol. 11, no. 21, 2588, 2019, doi: 10.3390/rs11212588.
[24] M. E. Hereher, "Estimation of Monthly Surface Air Temperatures From Modis LST Time Series Data: Application to the Deserts in the Sultanate of Oman," Environ. Monit. Assess., vol. 191, 592, 2019, doi: 10.1007/s10661-019-7771-y.
[25] USGS. Available online: https://earthexplorer.usgs.gov/ (accessed on 16 September 2024).
[26] J. D. Jang, A. A. Viau and F. Anctil, "Neural Network Estimation of Air Temperatures From AVHRR Data," *Int. J. Remote Sens.*, vol. 25, no. 21, pp. 4541-4554, 2004, doi: 10.1080/01431160310001657533.
[27] J. Hooker, G. Duveiller and A. Cescatti, "A Global Dataset of Air Temperature Derived From Satellite Remote Sensing and Weather Stations," Sci. Data, vol. 5, no. 1, 180246, 2018, doi: 10.1038/sdata.2018.246.
[28] B. Abbasi, Z. Qin, W. Du, J. Fan, S. Li and C. Zhao, "Spatiotemporal Variation of Land Surface Temperature Retrieved From FY-3D MERSI-II Data in Pakistan," Appl. Sci., vol. 12, no. 20, 10458, 2022, 10.3390/app122010458.

[29] P. Yu, T. Zhao, J. Shi, Y. Ran, L. Jia, D. Ji, and H. Xue, "Global Spatiotemporally Continuous Modis Land Surface Temperature Dataset," Sci. Data, vol. 9, no. 1, pp. 1-15, 2022, doi: 10.1038/s41597-022-01214-8.

[30] R. Olgun, C. Cheng and P. Coseo, "Nature-Based Solutions Scenario Planning for Climate Change Adaptation in Arid and Semi-Arid Regions," *Land*, vol. 13, no. 9, 1464, 2024, doi: 10.3390/land13091464.

[31] D. N. Bird, E. Banzhaf, J. Knopp, W. Wu, and L. Jones, "Combining Spatial and Temporal Data to Create a Fine-Resolution Daily Urban Air Temperature Product From Remote Sensing Land Surface Temperature (LST) Data. *Atmosphere*, vol. 13, no. 7, 1152, 2022, doi: 10.3390/atmos13071152.

[32] R. Olgun, N. Karakuş, S. Selim, T. Yilmaz, R. Erdoğan, M. Aklıbaşında, B. Dönmez, M. Çakır and Z. R. Ardahanlıoğlu. "Impacts of Landscape Composition on Land Surface Temperature in Expanding Desert Cities: A Case Study in Arizona, USA," *Land*, vol. 14, no. 6, 1274, 2025, doi: 10.3390/land14061274

[33] H. Nieto, I. Sandholt, I. Aguado, E. Chuvieco and S. Stisen, "Air Temperature Estimation With MSG-SEVIRI Data: Calibration and Validation of The TVX Algorithm for The Iberian Peninsula," *Remote Sens. Environ.,* vol. 115, no. 1, pp. 107-116, 2011, doi: 10.1016/j.rse.2010.08.010.

[34] A. Benali, A. Carvalho, J. Nunes, N. Carvalhais and A. Santos, "Estimating Air Surface Temperature in Portugal Using Modis Lst Data," *Remote Sens. Environ.*, vol. 124, pp. 108-121, 2012, doi: 10.1016/j.rse.2012.04.024.

[35] Y. Chen, J. Quan, W. Zhan and Z. Guo, "Enhanced Statistical Estimation of Air Temperature Incorporating Nighttime Light Data. *Remote Sensing*, vol. 8, no. 8, 656, 2016, doi: 10.3390/rs8080656.

[36] R. S. Dos Santos, "Estimating Spatio-Temporal Air Temperature in London (UK) Using Machine Learning and Earth Observation Satellite Data. *Int. J. Appl. Earth Obs. Geoinf.*, vol. 88, 102066, 2020, doi: 10.1016/j.jag.2020.102066.

[37] G. V. Mostovoy, R. L. King, K. R. Reddy, V. G. Kakani and M. G. Filippova, "Statistical Estimation of Daily Maximum and Minimum Air Temperatures From Modis LST Data Over The State of Mississippi," *GISci. Remote Sens.*, vol. 43, no. 1, pp. 78-110, 2006, doi: 10.2747/1548-1603.43.1.78.

[38] W. Zhang, B. Zhang, W. Zhu, X. Tang, F. Li, X. Liu and Q. Yu, "Comprehensive Assessment of Modis-Derived Near-Surface Air Temperature Using Wide Elevation-Spanned Measurements in China," *Sci. Total Environ.*, vol. 800, 149535, 2021, doi: 0.1016/j.scitotenv.2021.149535.

[39] B. Iqbal and M. Ali, "Estimation of Spatio-Temporal Air Temperature From Satellite Based LST Under Semi-Arid to Arid Environment in Peshawar Basin, Northwest Pakistan," *Adv. Space Res.*, vol. *70*, pp. 961-975, 2022, doi: 10.1016/j.asr.2022.05.052.

[40] A. Hurduc, S. L. Ermida and C. C. DaCamara, "On the Suitability of Different Satellite Land Surface Temperature Products to Study Surface Urban Heat Islands," *Remote Sensing*, vol. 16, no. 20, 3765, 2024, doi: 10.3390/rs16203765

[41] D. T. Gök, D. Scherler and H. Wulf, "Land Surface Temperature Trends Derived From Landsat Imagery in the Swiss Alps," *The Cryosphere*, vol. 18, pp. 5259-5276, 2024, doi: 10.5194/tc-18-5259-2024

[42] X. Ouyang, Z. Sun, S. Zhou and Y. Dou, "Urban Land Surface Temperature Retrieval With High-Spatial Resolution SDGSAT-1 Thermal Infrared Data," *Remote Sensing of Environment*, 312, 114320, 2024, doi: 10.1016/j.rse.2024.114320

[43] X. Wang, L. Zhong and Y. Ma, "Estimation of 30 m Land Surface Temperatures Over the Entire Tibetan Plateau Based on Landsat-7 ETM+ Data and Machine Learning Methods," *International Journal of Digital Earth*, vol. 15, no. 1, pp. 1038-1055, 2022, doi: 10.1080/17538947.2022.2088873

[44] W. Zhu, A. Lű and S. Jia, "Estimation of Daily Maximum and Minimum Air Temperature Using Modis Land Surface Temperature Products," *Remote Sens. Environ.*, vol. 130, pp. 62-73, 2013, doi: 10.1016/j.rse.2012.10.034.

[45] J. Cristóbal, M. Ninyerola, and X. Pons, "Modeling Air Temperature Through A Combination of Remote Sensing and GIS Data," *Journal of Geophysical Research: Atmospheres*, vol. 113, pp. 1-13, 2008, doi: 10.1029/2007JD009318

[46] M. Gholamnia, S. K. Alavipanah, A. Darvishi Boloorani, S. Hamzeh and M. Kiavarz, M, "Diurnal Air Temperature Modeling Based on the Land Surface Temperature," *Remote Sensing*, vol. 9, no. 9, 915, 2017, doi: 10.3390/rs9090915

[47] M. Burnett and D. Chen, "The Impact of Seasonality and Land Cover on the Consistency of Relationship between Air Temperature and LST Derived from Landsat 7 and MODIS at a Local Scale: A Case Study in Southern Ontario," *Land*, vol. 10, no. 7, 672, 2021, doi: 10.3390/land10070672

[48] D. J. Mildrexler, M. Zhao and S. W. Running, "A Global Comparison Between Station Air Temperatures and MODIS Land Surface Temperatures Reveals The Cooling Role of Forests," *Journal of Geophysical Research: Biogeosciences*, vol. 116, pp. 1-15, 2011, doi: 10.1029/2010JG001486

[49] İ. Cinar, N. Karakus and S. Toy, "Analysing Daytime Summer Thermal Comfort Conditions for Turkey's Third Largest Tourism Destination," *Environmental Science and Pollution Research*, vol. 30, no. 17, pp. 50046-50056, 2023, doi: 10.1007/s11356-023-25719-w

[50] N. Karakuş and E. Kahraman, "Uzaktan Algılama Verileriyle Arazi Kullanımı/Arazi Örtüsünün Arazi Yüzey Sıcaklığı Üzerindeki Etkisinin Değerlendirilmesi: Antalya Ili Konyaaltı Ilçesi Örneği," *Journal of Anatolian Environmental and Animal Sciences*, vol. 10, no. 6, pp. 1062-1069, 2025, doi: 10.35229/jaes.1804293

[51] B. Durmuş, İ. Bulut and B. Gönençgil, "Antalya Bölümünde Sıcaklık ve Yağış İndislerinin Değişim Analizleri," *Türk Coğrafya Dergisi*, vol. 78, pp. 91-108, 2021, doi: 10.17211/tcd.1009270

[52] Antalya Metropolitan Municipality. Available online: https://www.antalya.bel.tr/ (accessed on 9 March 2025).

[53] Haizea Analytics. Climate Zones on The Move. Available online: https://koppen.earth/ (accessed on 9 January 2026).

[54] TSMS. Turkish State Meteorological Service. Available online: https://www.mgm.gov.tr/veridegerlendirme/ (accessed on 13 February 2025).

[55] D. A. Artis and W. H. Carnahan, "Survey of Emissivity Variability in Thermography of Urban Areas, " *Remote Sensing of Environment*, vol. 12, no. 4, pp. 313-329, 1982, doi: 10.1016/0034-4257(82)90043-8

[56] J. A. Sobrino, J. C. Jiménez-Muñoz and L. Paolini, "Land Surface Temperature Retrieval From LANDSAT TM 5," *Remote Sensing of Environment*, vol. 90, no. 4, pp. 434-440, 2004, doi: 10.1016/j.rse.2004.02.003

[57] S. Roy, S. Pandit, E. A. Eva, M. S. H. Bagmar, M. Papia, L. Banik, T. Dube, F. Rahman and M. A. Razi, "Examining the Nexus Between Land Surface Temperature and Urban Growth in Chattogram Metropolitan Area of Bangladesh Using Long Term Landsat Series Data," *Urban Climate*, vol. 32, 100593, 2020, doi: 10.1016/j.uclim.2020.100593

[58] J. A. Sobrino, J. C. Jimenez-Munoz, G. Soria, M. Romaguera, L. Guanter, J. Moreno, A. Plaza and P. Martínez, "Land Surface Emissivity Retrieval From Different VNIR and TIR Sensors," *IEEE Transactions on Geoscience and Remote Sensing*, vol. 46, no. 2, pp. 316-327, 2008, doi: 10.1109/TGRS.2007.904834

[59] T. N. Carlson and D. A. Ripley, "On The Relation Between NDVI, Fractional Vegetation Cover, and Leaf Area Index," *Remote Sensing of Environment*, vol. 62, no. 3, pp. 241-252, 1997, doi: 10.1016/S0034-4257(97)00104-1

[60] D. Anandababu, B. M. Purushothaman and B. S. Suresh, "Estimation of Land Surface Temperature Using Landsat 8 Data," *International Journal of Advance Research*, vol. 4, no. 2, pp. 177-186, 2018.

[61] M. Stathopoulou and C. Cartalis, "Daytime Urban Heat Islands From Landsat ETM+ and Corine Land Cover Data: An Application to Major Cities in Greece," *Solar Energy*, vol. 81, no. 3, pp. 358-368, 2007, doi: 10.1016/j.solener.2006.06.014

[62] M. M. Salih, O. Z. Jasim, K. I. Hassoon and A. J. Abdalkadhum, "Land Surface Temperature Retrieval From LANDSAT-8 Thermal Infrared Sensor Data and Validation With Infrared Thermometer Camera," *International Journal of Engineering & Technology*, vol. 7, pp. 608-612, 2018, doi: 10.14419/ijet.v7i4.20.27402

[63] A. Şekertekin and A. M. Marangoz, "Zonguldak Metropolitan Alanındaki Arazi Kullanımı Arazi Örtüsünün Yer Yüzey Sıcaklığına Etkisi," *Geomatik*, vol. 4, no. 2, pp. 101-111, 2019, doi: 10.29128/geomatik.497051

[64] S. Prince, S. Goetz, R. Dubayah, K. Czajkowski and M. Thawley, "Inference of Surface and Air Temperature, Atmospheric Precipitable Water and Vapor Pressure Deficit Using Advanced Very High-Resolution Radiometer Satellite Observations: Comparison With Field Observations," *Journal of Hydrology*, vol. 212-213, pp. 230-249, doi: 10.1016/S0022-1694(98)00210-8

[65] C. Yoo, J. Im, S. Park and L. J. Quackenbush, "Estimation of Daily Maximum and Minimum Air Temperatures in Urban Landscapes Using MODIS Time Series Satellite Data," *ISPRS Journal of Photogrammetry and Remote Sensing*, vol. 137, pp. 149-162, 2018, doi: 10.1016/j.isprsjprs.2018.01.018

[66] T. Hengl, M. Nussbaum, M. N. Wright, G. B. M. Heuvelink and B. Gräler, "Random Forest As A Generic Framework For Predictive Modeling of Spatial and Spatio-Temporal Variables," *PeerJ*, vol. 6, e5518, 2018, doi: 10.7717/peerj.5518

[67] N. K. Malakar, G. C. Hulley, S. J. Hook, K. Laraby, M. Cook and J. R. Schott, "An Operational Land Surface Temperature Product For Landsat Thermal Data: Methodology and Validation," *IEEE Transactions on Geoscience and Remote Sensing*, vol. 56, no. 10, pp. 5717-5735, 2018, doi: 10.1109/TGRS.2018.2824828

[68] I. Agathangelidis, C. Cartalis and M. Santamouris, "Estimation of Air Temperatures for the Urban Agglomeration of Athens with the Use of Satellite Data," *Geoinfor Geostat: An Overview*, vol. 4, no. 2, pp. 1-7, 2016, doi: 10.4172/2327-4581.1000139

[69] X. Liu, Z. Cheng, L. Yan and Z. Yin, "Elevation Dependency of Recent and Future Minimum Surface Air Temperature Trends in the Tibetan Plateau and Its Surroundings," *Global Planet. Change*, vol. 68, no. 3, pp. 164-174, 2009, doi: 10.1016/j.gloplacha.2009.03.017.

[70] A. Hussain, J. Cao, I. Hussain, S. Begum, M. Akhtar, X. Wu, Y. Guan and J. Zhou, "Observed Trends and Variability of Temperature and Precipitation and Their Global Teleconnections in the Upper Indus Basin, Hindukush-Karakoram-Himalaya," *Atmosphere*, vol. 12, no. 8, 973, 2021, doi: 10.3390/atmos12080973.

[71] A. Gilbert and C. Vincent, "Atmospheric Temperature Changes Over the 20th Century at Very High Elevations in the European Alps from Englacial Temperatures," *Geophys. Res. Lett.*, vol. 40, no. 10, pp. 2102-2108, 2013, doi: 10.1002/grl.50401.

[72] S. F. Breitenbach, B. Plessen, S. Waltgenbach, R. Tjallingii, J. Leonhardt, K. P. Jochum, H. Meyer, B. Goswami, N. Marwan and D. Scholz, "Holocene Interaction of Maritime and Continental Climate in Central Europe: New Speleothem Evidence from Central Germany," *Global Planet. Change*, vol. 176, pp. 144-161, 2019, doi: 10.1016/j.gloplacha.2019.03.007.

[73] S. Piao, M. Cui, A. Chen, X. Wang, P. Ciais, J. Liu and Y. Tang, "Altitude and Temperature Dependence of Change in the Spring Vegetation Green-up Date From 1982 to 2006 in the Qinghai-Xizang Plateau," *Agric. For. Meteorol.*, vol. 151, no. 12, pp. 1599-1608, 2011, doi: 10.1016/j.agrformet.2011.06.016.

[74] F. Sariş, D. M. Hannah and W. J. Eastwood, "Spatial Variability of Precipitation Regimes over Turkey," *Hydrol. Sci. J.*, vol. 55, no. 2, pp. 234-249, 2010, doi: 10.1080/02626660903546142.

[75] İ. Çiçek, "Average Temperature Regimes of Selected Stations in Turkey," *Journal of Ankara University Research Center of Turkish Geography*, vol. 7, pp. 61-94, 1999.

[76] S. Selim, N. K. Sönmez and M. Çoşlu, *The Effect of Temporal Variation in Land Surface Temperature on Land Cover Classes and Agricultural Areas*. In Recent Studies in Planning and Design, 1st ed.; Altuntaş, A.; Alp, Ş., Ankara, Türkiye: IKSAD Publishing House, 2022.

[77] B. Efe, İ. Sezen, A. R. Lupo and A. Deniz, "The Relationship Between Atmospheric Blocking and Temperature Anomalies in Turkey Between 1977 and 2016," *Int. J. Climatol.*, vol. 40, no. 2, pp. 1022-1037, 2020, doi: 10.1002/joc.6253.

[78] D. Dong, G. Huang, X. Qu, W. Tao and G. Fan, "Temperature Trend-Altitude Relationship in China During 1963-2012," *Theor. Appl. Climatol.*, vol. 122, pp. 285-294, 2015, doi: 10.1007/s00704-014-1286-9.

[79] D. B. Enfield and L. Cid-Serrano, "Projecting the Risk of Future Climate Shifts," *Int. J. Climatol.*, vol. 26, no. 7, pp. 885-895, 2006, doi: 10.1002/joc.1293.

[80] S. M. Vicente-Serrano, J. I. López-Moreno, K. Correa, G. Avalos, J. Bazo, C. Azorin-Molina, F. Domínguez-Castro, A. El Kenawy, L. Gimeno and R. Nieto. Recent Changes in Monthly Surface Air Temperature over Peru, 1964-2014," *Int. J. Climatol.*, vol. 38, no. 1, pp. 283-306, 2017, doi: 10.1002/joc.5176.